Macromolecules

pubs.acs.org/Macromolecules Article

# Thermal Conduction and Phonon Transport in Folded Polyethylene Chains

Shibananda Das and Murugappan Muthukumar*

Cite This: *Macromolecules* 2023, 56, 393−403 Read Online

ACCESS | Metrics & More | Article Recommendations | Supporting Information

**ABSTRACT:** Using theory and simulations, we have investigated the phonons and their role in thermal energy transport in semicrystalline polyethylenes. Considering alternating stacks of lamellae and amorphous regions, and labeling one polyethylene chain interwoven among two amorphous regions and one lamella, we have explored the underlying mechanism of thermal conductivity of polyethylene in its semicrystalline state. We report that hairpin-like folds at the crystalline−amorphous interface significantly scatter phonons, allowing only less than half of the phonons to transmit through polyethylene backbone. Monitoring the phonon propagation and scattering at the interfaces, we have computed thermal conductivity of semicrystalline polyethylene. We have derived a design principle to control thermal conductivity of semicrystalline polyethylene in terms of lamellar thickness and the number of folds per chain at the crystalline−amorphous interface.

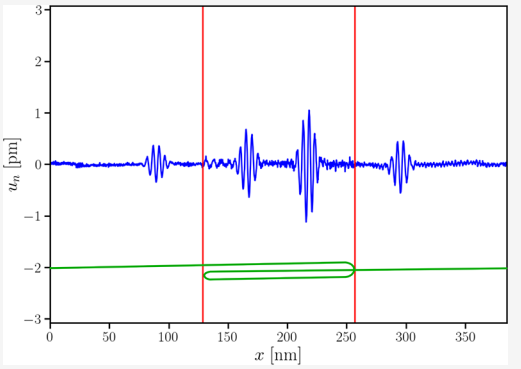




## INTRODUCTION

Bulk polymers are mostly utilized as thermal insulators because of ineffective heat conduction through them. In principle, the strong covalent bonds in the backbone of a polymer can efficiently conduct heat, but in the bulk condition due to entanglement of several chains the phonon vibrational energy dissipates through the interchain van der Waals interactions and thus results in a very low thermal conductivity. Polyolefin materials account for a high percentage of global thermoplastic production as they are lightweight, corrosion-resistive, and inexpensive to manufacture. A growing effort has been put toward improving their thermal conduction properties as this could be extremely beneficial for thermal management applications in industry, such as plastic heat exchangers, thermal interface materials, and packaging of electronics. A vast number of numerical[1−6] and experimental[7−10] studies have revealed ultradrawn polyethylene materials having higher thermal conductivities and in certain instances is even comparable to that of metals. In films and fibers, polyethylene is generally in a semicrystalline state containing multiple long, entangled, and folded lamellar chains with high structural anisotropy. It is well established now that mechanically stretching a polymer fiber or film improves the thermal conductivity by few orders of magnitude compared to their amorphous counterparts as the chain entanglements are significantly reduced and alignment of the chains is boosted. For example, the thermal conductivity of amorphous polyethylene at room temperature is roughly 0.2 W/(m K), whereas the thermal conductivity of an isolated fully stretched polyethylene (PE) chain has been reported to be as high as 350 W/(m K).[2] The experimental values of thermal conductivity are 104, 51, and 60 W/(m K) respectively for ultradrawn PE nanofibers,[8] commercial microfibers,[11] and PE films.[12,13]

Polyethylene in its semicrystalline form is a two-phase system consisting of alternating layers of ordered crystalline lamellar phase and disordered amorphous phase (Figure 1). In its simple form, the morphological period of such semicrystalline polymers is an amorphous interlamellar region sandwiched in the middle of two crystalline lamellar domains. Within the interlamellar regions, chains can adopt topologies of bridges, loops, and tails, as indicated in Figure 1. Chains passing through the interlamellar region and connecting the crystalline stems on both ends are the bridges. Segments of a single chain in the interlamellar region with their ends attached to the same lamella are loops. In a tail configuration, one end is connected to a lamellar stem and the other end terminates within the interlamellar region. These interlamellar chain topologies play a substantial role in determining the overall thermal conductivity and specifically bridges are the most important in efficient thermal transport.[14,15]

Theoretically, multiple models are available to describe the structure−property relationship in semicrystalline polymers under externally imposed strain and to predict their thermal

Received: September 21, 2022
Revised: November 23, 2022
Published: January 3, 2023





https://doi.org/10.1021/acs.macromol.2c01954
*Macromolecules* 2023, 56, 393−403

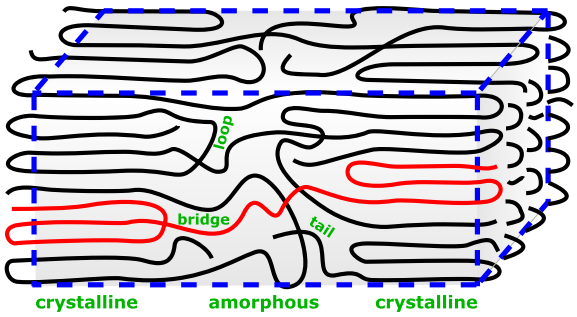


**Figure 1.** Schematic representation of a semicrystalline polyethylene showing two crystalline domains and the amorphous region sandwiched between them. Different types of chain topologies: bridges, loops, and tails, within the interlamellar amorphous region as labeled. The chain illustrated in red is a representation of one polyethylene conformation.

conductivity. The theoretical model proposed by Choy et al.[16] addresses the dependence of thermal conductivity on the crystallinity of semicrystalline polymers but underestimates the role of interlamellar bridges. Similarly, the widely used series model accounting the thermal resistances of the two phases in polyethylene materials undervalues the bridge topologies in the amorphous region.[17] A more sophisticated model proposed by Takayanagi et al.[18] incorporates the bridge chains and treats them as the same as the stems inside the crystalline lamellae. In particular, the bridges are considered to have the same thermal conductivity as the lamellar stems according to this model, such that thermal conductivity of the whole semicrystalline region depends on the width ratio of the region formed by the highly oriented bridges and the crystalline domain. Analogous to these analytical predictions, a few simulation studies have considered explicit semicrystalline sandwich structures containing various chain topologies within the interlamellar region.[14,15] These studies show that an increase in thermal conductivity of semicrystalline polymer fibers or films under mechanical stretching can be attributed to changes in the conformations of chains in their interlamellar region. The crystalline lamellae can break into several smaller crystalline regions, which are sandwiched by amorphous regions containing intrafibrillar bridge chains, with relatively small strains. These bridges extend, align themselves with increasing strain, and become the dominant medium of thermal energy transport.[15]

From a molecular point of view, one simplified consideration of the bridges is a polyethylene chain with hairpin-like folds forming lamellar stacks at the middle. The effects of structural disorders (curvature, kinks, and orientational disorder) at the molecular level on the thermal conductivity of polymer chains have been explored in the literature.[3,19−21] However, such a single-chain molecular level understanding of lamellar stacking and connecting bridges pertinent to the thermal transport is missing. Because such a chain configuration becomes prevalent during the stretching of a semicrystalline polyethylene as mentioned above, it is of fundamental interest to investigate the transport properties of chains with lamellar stacking.

In this paper, we consider configurations of a labeled polyethylene (PE) chain with hairpin folds forming lamellar domains and study the effect of such folds on their thermal transport properties. We report results of nonequilibrium molecular dynamics (NEMD) simulations characterizing the thermal boundary conductance/resistance of haipin-like folds depending on their conformational distribution along the polyethylene chain. We further analyze the effective thermal conductivity of the whole chain and its dependence on hairpin folds. Our study presents a detailed characterization of the role of interfaces formed by hairpin folds and bridge-like chains on thermal transport in polyethylene materials from a single chain molecular level and provides design algorithms to enhance thermal conductivity of semicrystalline polyethylenes.

## SIMULATION MODEL AND METHODS

We model the polyethylene chain as a united atom polymer, where each methylene group ($-CH_2-$) is represented by one single bead of mass $m$ = 14.0266 g/mol.[14,22] Our united atom model incorporates force fields to represent covalent bonds, backbone rigidity, and nonbonded van der Waals interactions. The bonded interactions for monomer connectivity are implemented by the harmonic potential

$$U_b = K(r - r_0)^2 \tag{1}$$

where $r$ is the distance between two neighboring monomers along the chain. The bond constant $K$ is taken as 450 kcal Å$^{-2}$ mol$^{-1}$, and the equilibrium bond length $r_0$ is 1.54 Å. The bending energy associated with the angle consisting of neighboring 3-bead fragment is described by

$$U_\theta = K_\theta(\theta - \theta_0)^2 \tag{2}$$

where the equilibrium bending angle $\theta_0$ = 109° and the bending rigidity $K_\theta$ = 60 kcal/mol. We also incorporate a multiharmonic potential given by[14,22]

$$U_\phi = K_1(1 + \cos\phi) + K_2(1 - \cos 2\phi) + K_3(1 + \cos 3\phi) \tag{3}$$

to model the chain stiffness arising from the torsional angle $\phi$ formed by the neighboring 4-bead fragment of the chain. The angle $\phi$ is defined according to the standard IUPAC sign convention. The stiffness parameters are taken as $K_1$ = 3.02 kcal/mol, $K_2$ = −0.56 kcal/mol, and $K_3$ = 2.58 kcal/mol.

We model the nonbonded van der Waals interactions with the following modified Lennard-Jones type potential

$$U_{nb} = \varepsilon\left[\left(\frac{\sigma}{r}\right)^{12} - 2\left(\frac{\sigma}{r}\right)^{6}\right] \tag{4}$$

where the interaction strength $\varepsilon$ is set to 0.112 kcal/mol. By following our earlier work,[22] the interaction for neighboring 3 beads along the polymer backbone is set to zero, and the equilibrium distance $\sigma$ is taken to be $\sigma$ = 4.53 Å for all the other interacting beads. The cutoff distance for the interaction is set to 2.5$\sigma$ in our simulations.

We performed molecular dynamics (MD) simulations to characterize the thermal properties of polyethylene chains. Because MD simulations are in the classical limit, we do a mapping of the temperature of a single PE chain from our simulations to that of a quantum phonon system to take into account quantum effects as in real systems. This is achieved by relating the total vibrational energy of the MD system to the quantum phonon system,[2,3,23,24] such that

$$T_{MD} = \frac{1}{3Nk_B}\int_0^\infty \hbar\omega g(\omega) f_{BE}(\omega, T)\, d\omega \tag{5}$$


https://doi.org/10.1021/acs.macromol.2c01954
Macromolecules 2023, 56, 393−403

Here, $T_{MD}$ and $T$ are the MD and the phonon system temperatures, $\hbar$ is the Planck constant divided by $2\pi$, $g(\omega)$ is the phonon density of state at frequency $\omega$, $f_{BE}(\omega,T)$ is the Bose−Einstein distribution, $k_B$ is the Boltzmann constant, and $N$ is the total number of repeat units per chain. From the preceding relation we find that a quantum phonon system with $T = 300$ K corresponds to $T_{MD} \approx 69$ K in our united atom MD system. All our simulations in the present paper to study the thermal properties of polyethylene have been performed at $T_{MD} = 69$ K.

We utilized the nonequilibrium molecular dynamics (NEMD) simulation approach to calculate the thermal conductivity of polyethylene chains. The thermal conductivity, $\kappa(L)$, of a system of finite length, $L$, is calculated according to the Fourier law as

$$\kappa(L) = \frac{J}{|\nabla T|} \tag{6}$$

where $J$ is the nonequilibrium steady-state heat flux and $\nabla T$ is the temperature gradient across the system. A thermal gradient is achieved by applying two different Langevin thermostats only at the two fixed ends of the system, where the ends are in contact with two reservoirs acting as heat source and sink as shown in Figure 2 for a single PE chain. The rest of the polymer chain is not considered to be in contact with any heat reservoir. The general equation of motion for all the monomer beads in a PE chain is given by


**Figure 2.** A polyethylene chain with fixed ends in contact with a heat source (red) and a heat sink (blue). This generates a temperature gradient across the chain represented by the color gradient.

$$m\frac{\mathrm{d}^2\mathbf{r}}{\mathrm{d}t^2} = \left(-m\gamma\frac{\mathrm{d}\mathbf{r}}{\mathrm{d}t} + \mathbf{\Gamma}\right) - \nabla U \tag{7}$$

Here, the first two terms inside the parentheses on the right-hand side are the fluctuation−dissipation terms of the Langevin thermostat, and these are taken to be zero for any monomer bead not part of thermostat regions. $\gamma$ denotes the friction coefficient, and thermal fluctuations are incorporated by the Gaussian white-noise vector $\mathbf{\Gamma}$, with $\langle\mathbf{\Gamma}\rangle = 0$, $\langle\mathbf{\Gamma}(t)\mathbf{\Gamma}(t')\rangle = 2m\gamma k_B T\mathbf{1}\delta(t-t')$, and $T$ the thermostat temperature. $-\nabla U$ indicates the conservative forces arising from all the potentials of a PE chain introduced above. The total heat flowing in $(Q_{hot})$ and out $(Q_{cold})$ of the two ends is accounted over time through the relation[25,26]

$$Q_{hot/cold}(t) = \int_{t_0}^{t}\left(-m\gamma\frac{\mathrm{d}\mathbf{r}}{\mathrm{d}t} + \mathbf{\Gamma}_{hot/cold}\right)\mathrm{d}\mathbf{r} \tag{8}$$

where $t_0$ is the initial time. We consider the system to be in steady state when the magnitudes of the accumulated heat flow in the two reservoirs are almost equal and there is an unchanged temperature profile. The steady-state heat flux $J$ between the heat source and sink is estimated from the heat accumulation rate, $\frac{\mathrm{dQ}}{\mathrm{d}t}$, using the relation

$$J = \frac{1}{S}\frac{\mathrm{dQ}}{\mathrm{d}t} = \frac{1}{2S}\left[\frac{\mathrm{dQ_{hot}}}{\mathrm{d}t} - \frac{\mathrm{dQ_{cold}}}{\mathrm{d}t}\right] \tag{9}$$

Here, $S$ is the cross-sectional area of the system in the transverse direction. Figure 3a shows the temperature profile across a polymer chain with the hot and cold ends (marked with red and blue colors) maintained at the temperatures 340 and 260 K, respectively. The corresponding average of heat accumulation/dissipation at heat sources/sinks are shown in Figure 3b as a function of time and the slope of the curve gives an estimate of $\frac{\mathrm{dQ}}{\mathrm{d}t}$ as defined in eq 9.

## RESULTS AND DISCUSSION

**Dispersion Curve and Thermal Conductivity of Unfolded PE Chains.** In MD simulations, interatomic force fields are crucial to precisely model phonon transport within a polyethylene chain. To validate our united atom PE model for the study of thermal conduction, we characterized the phonon properties of straight polyethylene chains. We considered an isolated fully stretched PE chain within a periodic simulation box of dimensions 64.19 nm × 9.24 nm × 9.24 nm, such that there is no interaction with periodic images in the transverse directions. Additionally, we also analyzed an orthorhombic

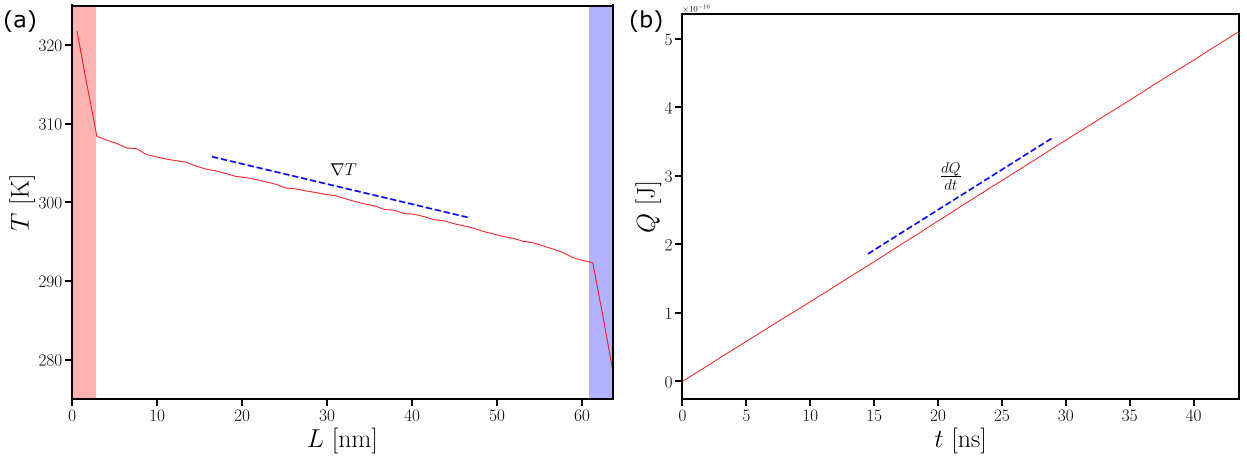


**Figure 3.** (a) Temperature profile along a 65 nm polyethylene chain with a steady state heat flux. The slope of the profile gives the temperature gradient $\nabla T$. (b) Total input energy, $Q$, in the thermostat regions as a function of time. The heat accumulation rate, $\mathrm{d}Q/\mathrm{d}t$, is calculated from the slope.



https://doi.org/10.1021/acs.macromol.2c01954
Macromolecules 2023, 56, 393−403

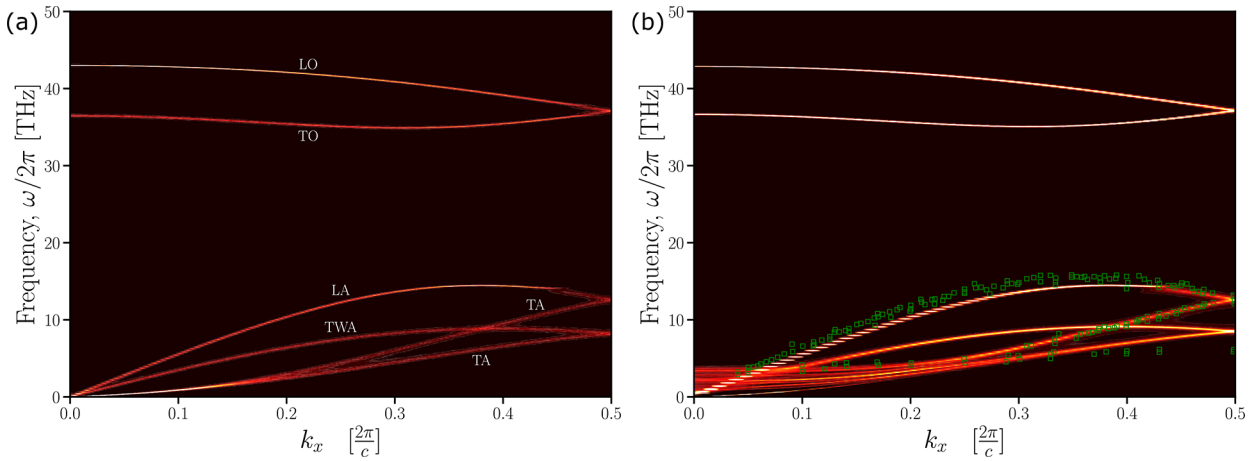


**Figure 4.** Phonon dispersion curves as a function of frequency, $\omega$, and wavevector, $k_x$, in the longitudinal direction of (a) a single unfolded PE chain and (b) an orthorhombic crystal of 24 PE chains calculated from our united atom model. $c$ here is the size of one unit cell of PE. Green squares are the inelastic neutron scattering data from experiments for the longitudinal [Adapted from ref 32.] and transverse acoustic modes. [Adapted from ref 33. Copyright 2002 Royal Society of Chemistry.] LA, TA, and TWA are the longitudinal, transverse, and torsional acoustic polarizations. LO and TO are the longitudinal and transverse optical polarizations.

crystal of 24 PE chains within a periodic simulation box of dimensions 32.09 nm × 1.8 nm × 2.32 nm. In both cases, we first equilibrated the systems by performing NVT simulations, and then we collected our data to determine phonon properties by doing simulations in NVE ensemble for 90 ps.

We determine the phonon dispersion curves by calculating the spectral energy density as a function of angular frequency, $\omega$, and wavevector, $k_x$, in the longitudinal direction. The spectral energy density is defined as two-dimensional Fourier transform of the velocity of one certain bead in a unit cell of PE:[4,27−30]

$$\Phi(\omega, k_x) = \frac{m}{4\pi\tau_0 p N_c} \sum^{p} \sum^{\alpha} \left| \int \sum_{n=1}^{N_c} v_\alpha(x_n, t) e^{i(k_x x_n - \omega t)} \, dt \right|^2 \tag{10}$$

Here, $N_c$ is the number of unit cells with a size $c$ = 0.251 nm in the longitudinal $x$-direction, $p$ is the number of monomer beads per unit cell, $\tau_0$ is the total integration time, $m$ is the mass of a methylene group, and $\alpha = \{x, y, z\}$. We extract the frequencies corresponding to the peak values of the spectral energy density at different wave vectors. Thus, we obtain the characteristic frequencies for each wave vector or the dispersion relation. Our calculated phonon dispersion for a stretched single PE chain is shown in Figure 4a. Our model can capture the longitudinal, transverse, twisting acoustic phonon modes and also the longitudinal, transverse optical modes. The dispersion curves are in reasonable agreement with the first-principles-based anharmonic lattice dynamics calculations[31] and also with other numerical studies.[2−4] Figure 4b shows the dispersion curves of 24 lamellar PE chains arranged in an orthorhombic crystal and is compared with experimental data for the longitudinal and transverse acoustic modes.[32,33] Our phonon dispersion showing similar groups of acoustic phonon branches as in experiments at lower frequencies validates that our relatively simple united atom model can accurately describe PE phonon dynamics and is an appropriate model to calculate thermal conductivity. It is clear that the acoustic phonons are the main contributors to phonon transport and thermal conduction due to their large group velocity $\left(v_g = \frac{d\omega}{dk}\right)$. Moreover, we can observe that the dispersion curves of the longitudinal acoustic (LA) mode are the same for the single chain and the crystal. The only significant difference is evident for the curves belonging to the transverse acoustic (TA) mode. This is expected as phonon vibration in the transverse direction gets hindered with the presence of surrounding chains, but the longitudinal vibrations are unaffected.

Previous studies in the literature have shown a strong dependence of the thermal conductivity on the length of the polymer chains.[1−3] We characterize the length dependence of thermal conductivity (TC) for our model by varying the length of polyethylene for the single chain case and also for orthorhombic fibers consisting of 7 polyethylene chains. The thermal conductivity of a single chain obtained from our simulations is plotted in Figure 5 (red curve) as a function of chain length. We observe a power-law dependence of the thermal conductivity on the chain length with an exponent of about 0.488 above a certain chain length and is in accordance with the literature.[34] For much smaller chains, the length is comparable to the phonon mean free path (MFP), and as a

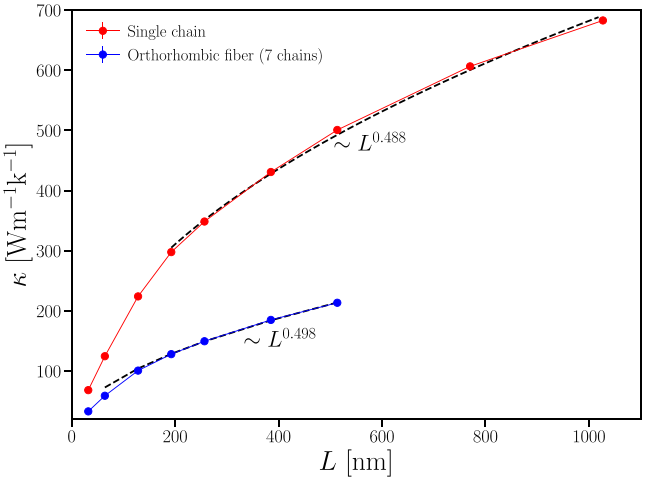


**Figure 5.** Thermal conductivity as a function of the chain length for single straight polyethylene chains (red) and orthorhombic polyethylene fibers consisting of 7 chains (blue) at $T$ = 300 K. The black dashed lines are power-law fits to the data.


https://doi.org/10.1021/acs.macromol.2c01954
Macromolecules 2023, 56, 393−403

result, we observe almost a linear dependence of TC on the chain length $L$. The blue curve in Figure 5 corresponds to PE fiber, where we consider 7 different fiber lengths assembled with the orthorhombic crystal symmetry. The thermal conductivity value in this case is much lower than that in a single chain. This is expected as the phonon vibrational energy dissipates through interchain van der Waals interactions in the transverse directions in the presence of surrounding chains. The power-law dependence of the thermal conductivity in this case has an exponent of about 0.498.

**Hairpin-like Folds in PE Chain.** For PE chains with hairpin-like folds, we consider many different configurations characterized in terms of the number of lamellar stacks ($N_{lamella}$), number of stems in each lamella stack ($N_{stem}$), uniform length of the stems ($L_{stem}$), and the overall end-to-end length of the whole chain ($L$). Figure 6 shows the simplest

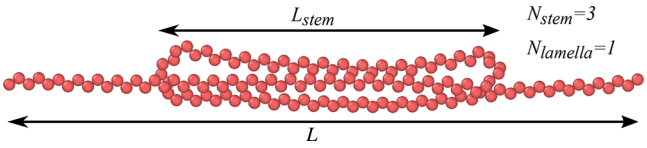


**Figure 6.** Snapshot of a lamellar domain consisting of three stems formed by a single polyethylene chain with two hairpin folds and two end-strands in the amorphous domains. Such a conformation is characterized by the number of lamellar stacks ($N_{lamella}$), number of stems in each lamella stack ($N_{stem}$), length of the stems ($L_{stem}$), and the overall end-to-end length of the whole chain ($L$).

scenario of three lamellar stems formed in a PE chain with two hairpin folds and the two ends in the interlamellar region. We investigate the thermal transport properties of such PE chain configurations by controlling the various conformational parameters.

Figure 7a shows the temperature profile across a PE chain comprising of two hairpin-like folds in the middle, where the two ends are maintained at the temperatures 360 and 240 K. In the presence of a steady heat flux, we observe significant temperature jumps $\Delta T$ at the interfaces of the two hairpin-folds and a slight temperature gradient in the middle lamellar segment. The temperature jumps are an interesting phenomenon which is noticed near interfaces during thermal transport and is generally interpreted in terms of thermal boundary resistance (TBR).[35,36] The thermal resistance of an interface, also termed the Kapitza resistance, represents a barrier associated with the heat transport across it. This originates from the differences in the phonon spectra of the two phases separated by the interface, which leads to scattering of thermal energy or phonons and a discontinuity in the temperature develops at the interface in the presence of a heat flux. Such temperature jumps have previously been observed in polyethylene chains in the presence of kinks along the backbone.[3] A similar temperature profile and discontinuities also appear near the crystalline−amorphous interface in semicrystalline polyethylene, when it is stretched under the effect of strains.[15] We varied the stem lengths of the middle segment (not shown here) and found that the temperature gradient in the middle part disappears for smaller stems. From our observations in Figure 5, we know that the thermal conductivity transitions toward a linear dependence of $L$ for single chains and fibers in those smaller length limit ($L_{stem} \ll 30$ nm). A nonlinear dependence can be expected only when the sample length is few orders higher than the phonon MFP. Thus, it is reasonable that for very small stem lengths (comparable to the phonon MFP) ballistic transport of phonon dominates instead of diffusive one, which results in an uniform temperature profile in the lamella. Figure 7b shows the phonon density of states, $g(\omega)$, of the hairpin chain calculated from the Fourier transform of the velocity autocorrelation function averaged over all monomers as[24,27,37]

$$g(\omega) = \frac{Nm}{3k_BT}\int \langle \mathbf{v}(t)\cdot\mathbf{v}(0)\rangle e^{i\omega t}\, dt \tag{11}$$

where $N$ is the total number of monomers. The phonon density of states for the hairpin chain configuration exhibits an additional peak at about 2.5 THz compared to a single stretched chain (Figure 7c). This low-frequency peak is more prominent for an orthorhombic fiber consisting of 7 chains as shown in Figure 7d. Additional data for the dependence of the phonon density of states on $N_{\text{lamella}}$, $N_{\text{stem}}$, and $L_{\text{stem}}$ are provided in the Supporting Information. The changes to $g(\omega)$ with an additional peak at 2.5 THz due to the crystalline−amorphous interface are expected, consistent with the discontinuities observed in the temperature profile (Figure 7a).

We characterize the interfaces formed by the hairpin-like folds in a polyethylene chain in terms of the thermal boundary conductance (inverse of TBR), which is related to the temperature drop across the interface and is estimated as

$$G = \frac{J}{\Delta T} \tag{12}$$

where $\Delta T$ is the temperature jump near a hairpin interface. For this expression, it is generally assumed that there is no inelastic phonon scattering at the interface. For the system shown in Figure 7, we get a thermal boundary conductance of 325 MW/($m^2$ K) corresponding to the temperature jumps near the hairpin folds. Additionally, many analytical theories estimate the thermal boundary conductance (TBC) by considering a net heat flux across the interfacial junction in steady-state. For equilibrium phonon distribution the general expression for TBC is given by[38,39]

$$G = \frac{1}{V}\sum_{\nu,\mathbf{k}}^{+} \hbar\omega v_x \alpha_{L\to R}\frac{df_{BE}}{dT} \tag{13}$$

where $\omega$ is the frequency of a phonon normal mode with polarization $\nu$, $\mathbf{k}$ is the phonon wave vector, and $v_x$ is the component of the phonon group velocity perpendicular to the interface plane. The plus sign on the summation indicates that only the modes with positive group velocity are included. $\alpha_{L\to R}$ is the mode-dependent phonon transmission coefficient, defined as the fraction of the incident phonon energy that is transmitted from the left side to the right side of the interface, and is a critical factor determining the thermal resistance/conductance of an interface.

The nonequilibrium phonon wave packet method proposed by Schelling et al.[40] is frequently used in simulation studies to understand the interfacial phonon transport properties and to estimate the phonon boundary transmission. This technique has been employed in studies of phonon scattering at ideal interfaces, grain boundaries, rough surfaces, Lennard-Jones solids, semiconductors, carbon nanotubes, and polymers.[40−43] To characterize and obtain an in-depth understanding of the phonon scattering mechanism across the interface of hairpin folds in our system, we adopt this method. The fundamental idea is to create a localized Gaussian wave envelope from a


https://doi.org/10.1021/acs.macromol.2c01954
Macromolecules 2023, 56, 393−403

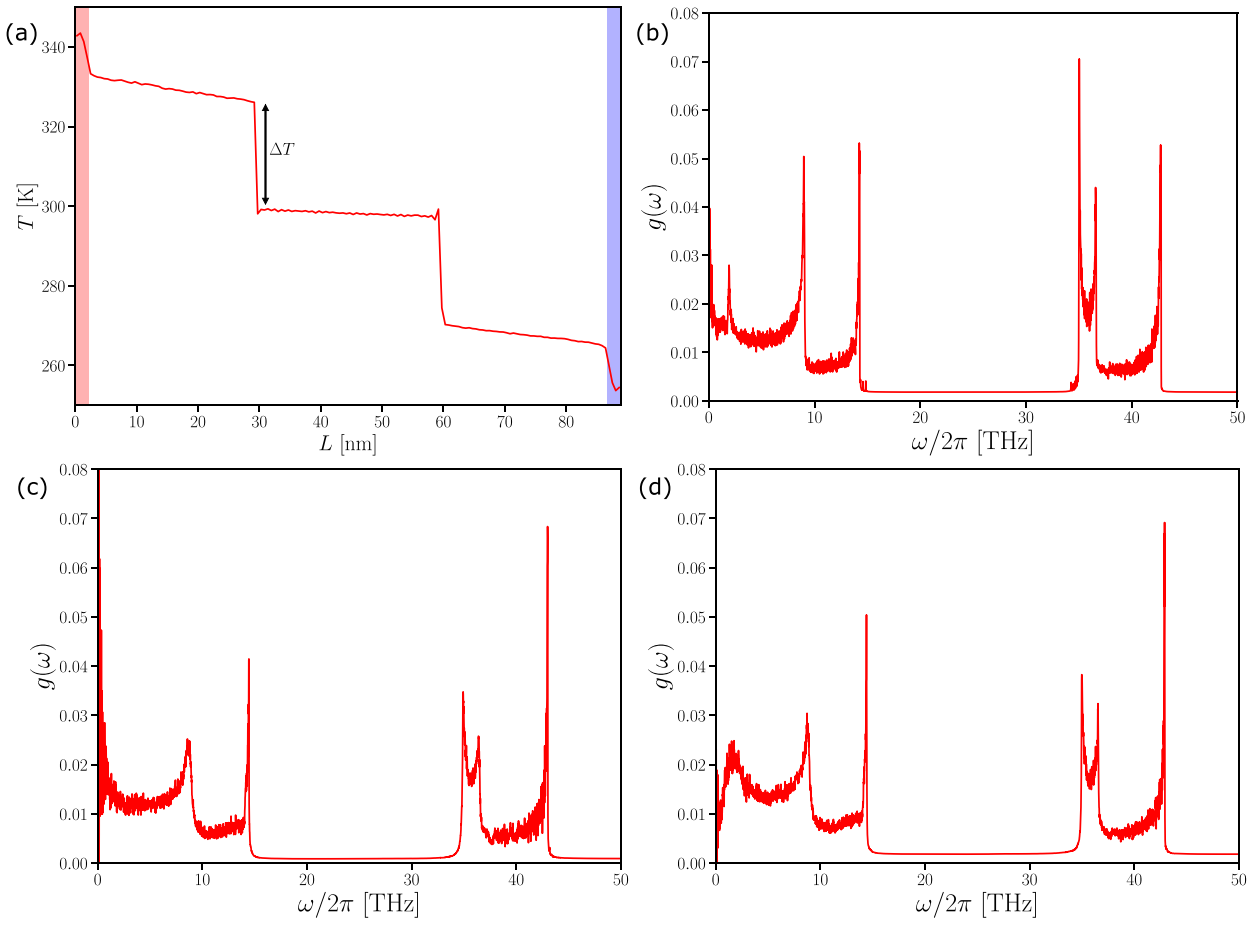


**Figure 7.** (a) Steady-state temperature profile across a polyethylene chain comprising of two hairpin-like folds ($N_{stem}$ = 3) and end-to-end length, $L$ ~ 88 nm. The two discontinuities ($\Delta T$) in the temperature are at the position of the two folds. (b) Corresponding phonon density of states for this configuration of the chain consisting of 3 stems in a lamella. Phonon density of states of (c) a single stretched PE chain and (d) an orthorhombic fiber consisting of 7 PE chains.

single branch of the phonon dispersion curve with a well-defined polarization, which is then allowed to propagate. A Gaussian wave packet is generated for each phonon mode by assigning an appropriate displacement $\mathbf{u}_n$ for the nth monomer

$$\mathbf{u}_n = A\boldsymbol{\nu}(k_x)\exp\{i[k_x(x_n - x_0) - \omega t]\} \times \exp[-(x_n - x_0)^2/2\xi^2] \quad (14)$$

Here, $A$ is the displacement amplitude, $\mathbf{v}(k_x)$ is the polarization vector, $x_0$ is the initial position of the wave packet, $x_n$ is the position of the $n$th monomer, and $\xi$ is the standard deviation of the wave packet. The velocity of a monomer in the wave packet is given by

$$\mathbf{v}_n = \frac{\partial u_n}{\partial t} = -i\omega u_n \quad (15)$$

We obtain the initial displacement and velocity of the monomers by setting $t$ = 0 in the preceding expressions. The kinetic energy in the chain is removed completely to make the monomers to be around their equilibrium positions. Then the wave packet displacement and velocities are introduced, and the chain is allowed to evolve over time using NVE MD simulation. We consider a chain similar to Figure 6 with periodic boundaries at the ends. Then a Gaussian wave packet with initial amplitude $A$ = 1.25 pm and $\xi$ = 5.01 nm is placed at the end of the simulation box. We consider the longitudinal mode such that $\mathbf{v}(k_x) = (1,0,0)^T$. The wave vector $k_x$ and the corresponding frequency $\omega$ are varied according to the dispersion relation. Figure 8 shows propagation of the LA phonon wave packet with $k_x = 0.05\left(\frac{2\pi}{c}\right)$ and frequency $\omega$ = 2.785 THz. Because the chain stretches along the $x$-axis in our simulations, we obtain the LA wave packet by calculating the displacements of the monomers in the $x$-direction with respect to their equilibrium positions. At any section of the folded chain, we report the resultant displacement of all the monomers belonging to that particular unit cell. We observe that the initial wave packet breaks up into a right-moving and a left-moving waves denoted as **1** and **2**, respectively (Figure 8a). As shown in Figure 8b,c, these smaller waves cross each other and continue moving along the straight parts of the chain until they encounter the kinks (monomers in gauche state) at the hairpin folds (positions denoted by the red vertical lines). Elastic scattering at the interfaces results in a transmitted wave (**1′** and **2′**) and a reflected wave (**1** and **2**) both at the frequency $\omega$ (Figure 8d). This scattering phenomenon leads to the discontinuities in the temperature, shown in Figure 7a. We determine the phonon transmission coefficient $\alpha$ by calculating the ratio between the amplitudes of transmitted ($A_{tr}$) and initial ($A$) phonon wave packets as


https://doi.org/10.1021/acs.macromol.2c01954
Macromolecules 2023, 56, 393−403

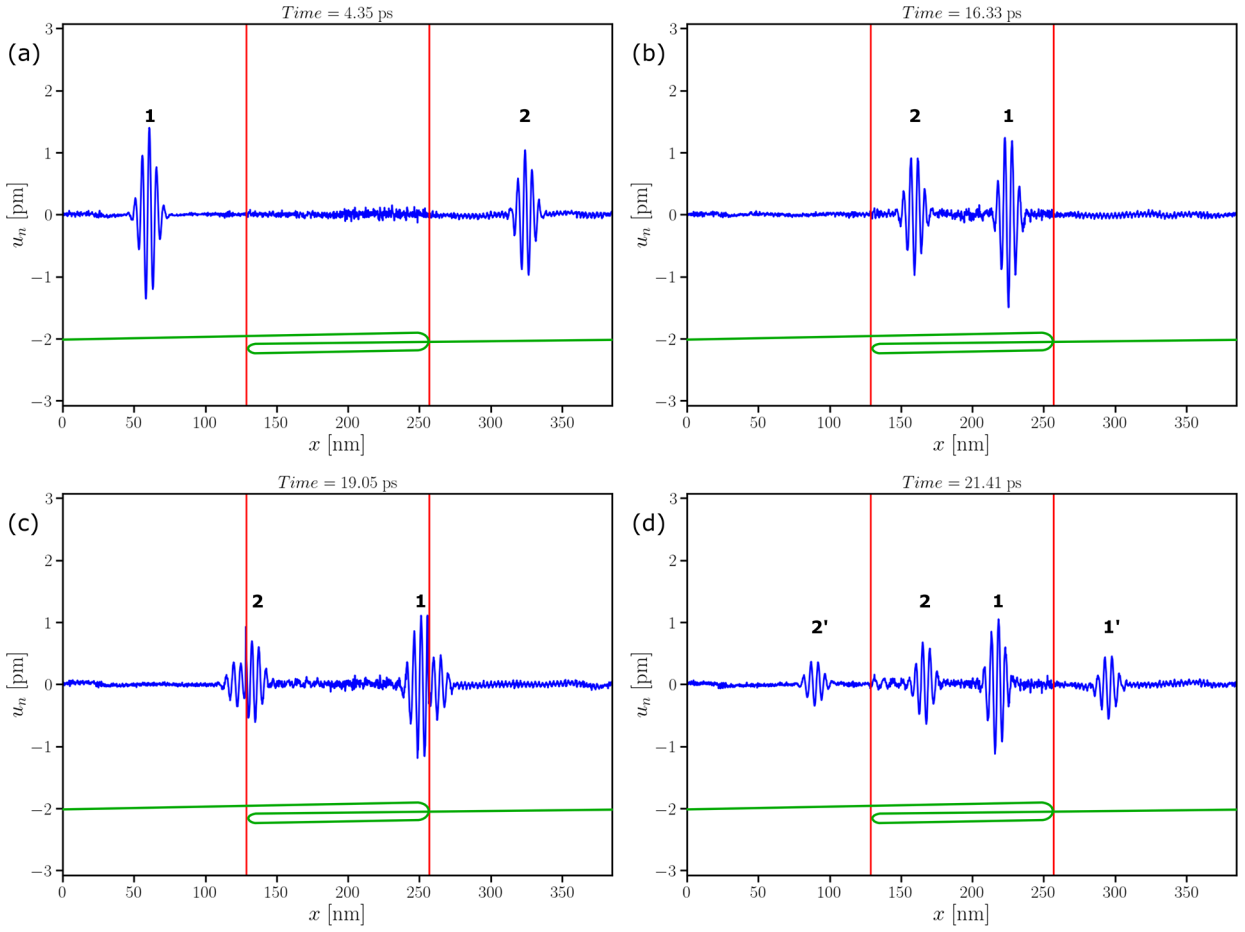


**Figure 8.** Evolution of a LA phonon wave packet [$k_x = 0.05(2\pi/c)$, $\omega = 2.785$ THz] in a PE chain with periodic boundaries and the structural parameters $N_{lamella} = 1$ and $N_{stem} = 3$. (a) Initially the wave packet is placed at the end of the simulation box, which breaks down into smaller waves **1** and **2** ($t = 4.35$ ps). (b) Waves continue to move along the straight parts of the PE chain passing the interface without any scattering ($t = 16.33$ ps). (c) Waves encounter the hairpin folds or monomers in gauche state ($t = 19.05$ ps). (d) Waves are scattered into a transmitted wave (**1**′ and **2**′) and a reflected wave (**1** and **2**) both at the frequency $\omega$ ($t = 21.41$ ps).

$$\alpha = \left(\frac{A_{tr}}{A}\right)^2 \tag{16}$$

Figure 9 shows the phonon transmission coefficient for the LA mode across a hairpin fold in the PE chain calculated using the phonon wave packet method. Within the low frequency range (<10 THz) considered here, the group velocity of these longitudinal acoustic phonons decreases with increasing frequency, and thus, the phonon transmission probability decreases monotonically.

We have investigated the effect of polymer conformation with hairpin folds in detail by varying the stem lengths of the middle segment (for $N_{lamella} = 1$, $N_{stem} = 3$) and also the number of hairpin folds (or $N_{stem}$). Figure 10a shows TBC for a system with two folds and three stems in the middle segment, where $L_{stem}$ is varied keeping the length of the end segments the same. We consider two Langevin heat reservoirs for the two ends maintained at the temperatures 360 and 240 K to estimate the TBC using eq 12. We find an increase in thermal boundary conductance with increasing stem length. Generally, TBC depends on the interface shape and width and the thermal conductivities of the domains on both sides of the interface. From our previous considerations of straight chains, we know that increasing the length of the chain increases the thermal conductivity for a bundle of multiple chains (see Figure 5). As the length of the stems in Figure 10a is increased, the thermal conductivity of the lamellar segment also increases

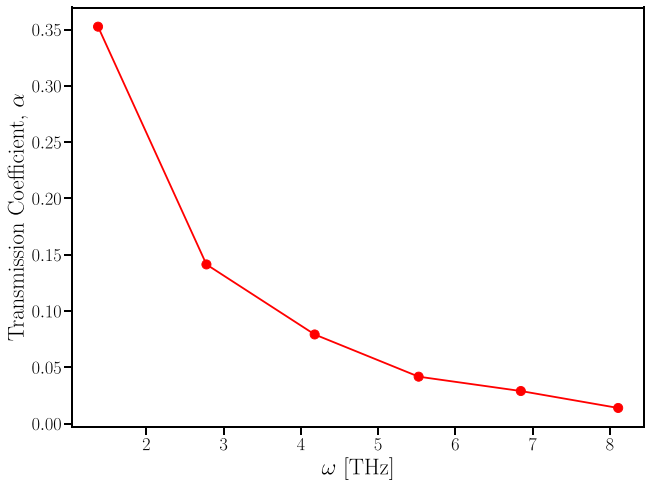


**Figure 9.** Phonon transmission coefficient for the longitudinal acoustic mode measured from the transmission amplitudes of a Gaussian wave packet with initial amplitude $A = 2.5$ pm and $\xi = 5.01$ nm. The wave vector $k_x$ for the corresponding frequency $\omega$ is varied according to the dispersion relation.



https://doi.org/10.1021/acs.macromol.2c01954
Macromolecules 2023, 56, 393−403

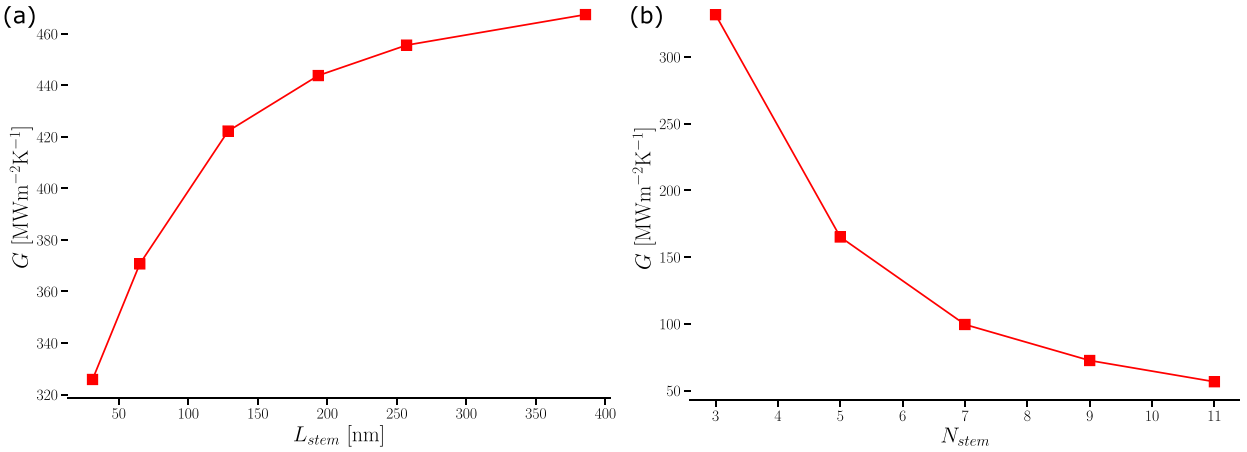


**Figure 10.** (a) Thermal boundary conductance (TBC) for systems with two hairpin-like folds ($N_{lamella}$ = 1, $N_{stem}$ = 3) as the stem length, $L_{stem}$, in the lamella is increased. (b) TBC for systems with different number of hairpin-like folds such that $N_{stem}$ changes ($N_{lamella}$ = 1) and the end-to-end chain length is fixed.

accordingly, and there is less thermal conductivity difference between the two segments across the hairpin interface. Thus, we expect that the TBC of the interface increases with increasing stem length as shown in Figure 10a. In terms of phonon transmission, it indicates that more phonons are transmitted across the hairpin interface improving the thermal boundary conductance. In Figure 10b, we also find that the TBC monotonically decreases with an increase in the number of hairpin folds or $N_{stem}$ in the lamellar stack, while the end-to-end length of the whole polymer is fixed. This is due to the broader interface leading to higher phonon scattering and less phonon transmission across it. In analogy with the semicrystalline polymer interfaces, larger the interface compared to the width of the bridge chains higher would be the thermal resistance.

The effective thermal conductivity, $\kappa_{eff}$, of the whole chain from the left end to the right end can be calculated using eq 6 for all the different chain conformations considered above, where $|\nabla T|$ is estimated as the ratio of the temperature difference across the both ends and the end-to-end length of the whole chain. Following series thermal resistor model, we also consider the effective thermal conductivity of the whole chain as $\kappa_s = L/R_{total}$. $R_{total}$ is the sum of the thermal resistance of the various segments and the hairpin interface in a chain, given by

$$R_{total} = N_s R_{chain} + (N_s - 1)R_{stem} + 2(N_s - 1)R_{fold} \quad (17)$$

Here, $N_s$ is the number of single chain segments and $R_{chain}$ is the corresponding estimated resistance. Similarly, the resistance of the multistem segments is $R_{stem}$ and the resistance of the interface is $R_{fold}$. We estimated the three different resistances by calculating the local thermal conductivities of the various single chain and lamellar segments and the thermal boundary conductance of the hairpin interfaces. Figure 11 shows the effective thermal conductivity of the whole chain calculated via the direct method ($\kappa_{eff}$) and also considering series resistance ($\kappa_s$). We take into account changes in the chain conformation through the two different approaches considered above, namely, varying the stem length and changing the number of stems. We combine these two approaches together in one single plot by defining the fold factor, $f_{hf} = \frac{\sqrt{N_{stem}}\sigma}{L}$, which is the ratio of the width of the multistem segment to the end-to-end length of the chain.

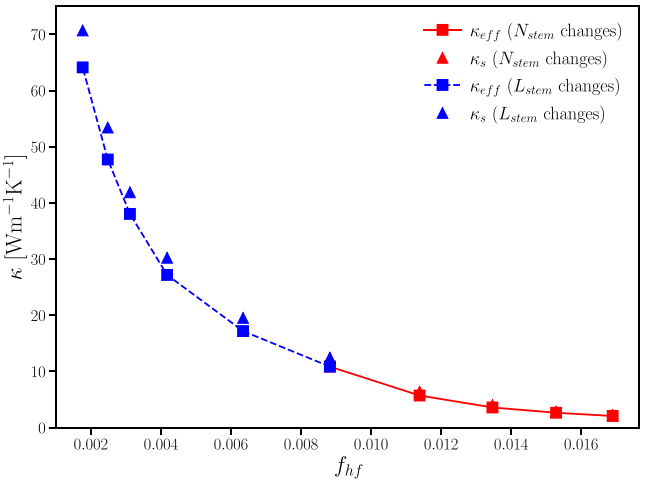


**Figure 11.** Effective thermal conductivity $\kappa_{eff}$ (squares) and $\kappa_s$ (triangles) as a function of fold factor, $f_{hf} = \frac{\sqrt{N_{stem}}\sigma}{L}$, which is the ratio of the width of the multistem segment to the end-to-end length of the chain. The thermal conductivity values from the stem length variation is colored blue and the ones with stem number variation is colored red.

Interestingly, for $N_{lamella}$ = 1, all the thermal conductivity data fall into one continuous curve when plotted as a function of $f_{hf}$. Because we consider one single bridge-like chain protruding out of each end of the lamella, increasing $f_{hf}$ by increasing $N_{stem}$ represents an increase in the relative area per chain at the interface. Thus, for a fixed number of bridge chain, the fold factor in our system is equivalent to the width ratio of bridge-topology chains addressed in the Takayanagi model.[14,18] We find that the effective thermal conductivity decreases at higher fold factors or with an increasing fraction of the amorphous component of the single chain segments for a fixed end-to-end length (analogous to bridges in semicrystalline polyethylene) as expected from the Takayanagi model. This shows the importance of the fraction of bridges in semicrystalline polyethylene compared to crystalline stems in deciding the thermal conductivity. We also observe a reasonable agreement between the effective thermal conductivity, $\kappa_{eff}$, and the estimation, $k_s$, considering a simple series thermal resistance


https://doi.org/10.1021/acs.macromol.2c01954
Macromolecules 2023, 56, 393−403

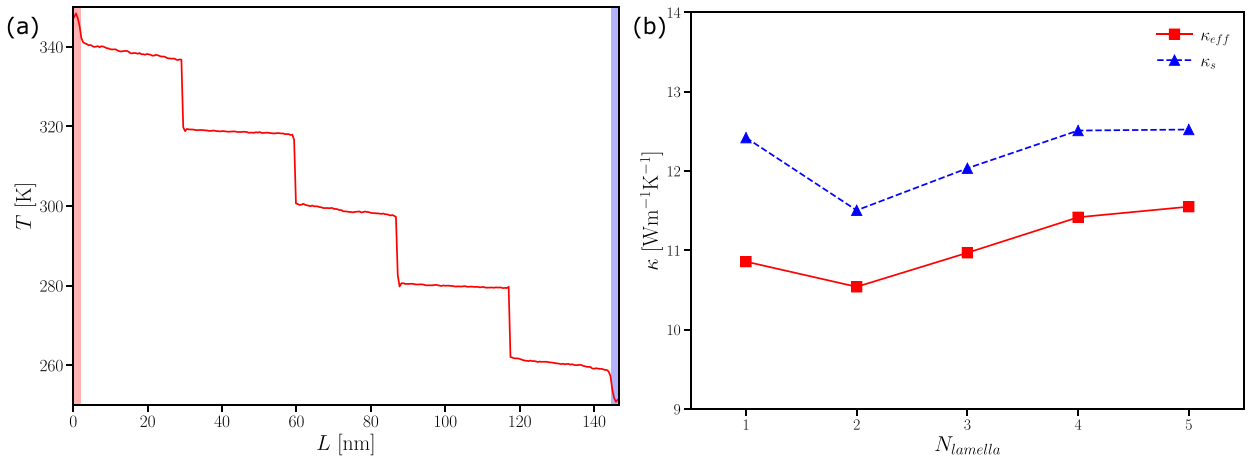


**Figure 12.** (a) Temperature profile across a system of polyethylene chain with two lamella ($N_{lamella}$ = 2) each consisting of two hairpin folds ($N_{stem}$ = 3). (b) Effective thermal conductivity $\kappa_{eff}$ (red squares) and $\kappa_s$ (blue triangles) as a function of the number of lamellar stacks, $N_{lamella}$, with $N_{stem}$ = 3.

model with only a difference of <13%. Overall, we identify a strategy to improve the thermal conductivity by either increasing the lamellar stem length or reducing the interfacial width per chain, as both conditions lead to lower thermal boundary resistance. In terms of comparison between our predictions and experiments, thermal conductivity generally depends on a lot of factors under experimental situations, e.g., the amount of crystallinity, external strains, etc. Experiments have reported values of the TC between 10 and 100 W/(m K) under varying conditions. Thus, for highly ordered semicrystalline polyethylene the thermal conductivity values as in our simulations are of the same order as experimental observations and also the trend in effective TC is as expected. Then again, our results are not directly comparable with experiments since we consider one isolated chain with hairpin folds, instead of explicit crystalline and amorphous domains of multiple chains.

In Figure 12, we consider the system of multiple lamella with two hairpin folds along the polymer chain (fixed $N_{stem}$ = 3 and $L_{stem}$ = 30 nm, while $L$ changes). This is a single chain representation of semicrystalline polymer with multiple crystalline domains connected via bridge chains, specifically under high mechanical strain.[15] From the temperature profile for a chain with two lamella in Figure 12a, we observe the same temperature jumps at all fold interfaces. We have calculated the effective thermal conductivity with increasing $N_{lamella}$ following both the direct and the series resistance method. We find that the effective thermal conductivity is essentially independent of the number of lamella with two hairpin folds, and the difference between the values from the two approaches is <13%, as shown in Figure 12b. The constant value of thermal conductivity is because the ratio of the number of lamella and the end-to-end is roughly the same in all the cases. In conformity with Figure 11, which shows that the relative area per chain at the interface, i.e., the bridge to stem width ratio, of the lamella is an important factor, we find that the thermal conductivity in chains with multiple identical lamella is essentially the same as with one single lamella. Thus, the determination of the thermal conductivity of a semicrystalline polyethylene material using simulations can be simplified by addressing only one of the repeating sandwich structures with crystalline lamella at the sides and the amorphous interlamellar region in the middle.

## SUMMARY AND CONCLUSIONS

In conclusion, we have studied in detail the effect of hairpin-like folds on the thermal transport properties by treating the semicrystalline polyethylene with bridges in terms of a simplified consideration of a single chain with hairpin-like folds forming lamellar stacks. Such a single chain representation is relevant to semicrystalline polyethylene systems under moderate levels of externally imposed strain. In particular, we have varied the lamellar thickness and the number of stems per chain in the lamellae to characterize the thermal boundary conductance at the interface of hairpin-like folds and the single stem ends. We observe temperature jumps at the interfaces formed by the hairpin-like folds due to phonon scattering. The phonon scattering amplitudes have been calculated using wave packet simulations, which reveal significant scattering at the hairpin folds with only about one-third of the longitudinal acoustic phonons being transmitted. We present an estimation of the effective thermal conductivity of the whole chain, which reveals that both the chain length and the relative cross-sectional width of the hairpin folds per chain at the crystalline−amorphous interface are the critical factors. The thermal conductivity of the chain decreases with an increase in the number of stems or a decrease in the length of the stems in the crystalline domain for the same fixed number of bridges. Finally, we find that in a system with multiple identical periods of lamellar stacks and bridges, thermal conductivity calculations can be simplified by considering only one period. Overall, our study reveals molecular details of how thermal energy transports across the crystalline−amorphous interface at a single chain level. An obvious future extension of this study is to investigate the phonon scattering and thermal energy relaxation in semicrystalline polyethylenes where the amorphous region is entangled with multiple interpenetrating bridge chain segments and to quantify the entropy production due to interchain phonon scattering inside amorphous domains.

## ASSOCIATED CONTENT

### Supporting Information

The Supporting Information is available free of charge at https://pubs.acs.org/doi/10.1021/acs.macromol.2c01954.

Phonon density of states for different conformational variations of folded polyethylene chains. Character-



https://doi.org/10.1021/acs.macromol.2c01954
Macromolecules 2023, 56, 393−403

ization of the evolution of a LA phonon wave packet in a stretched chain (PDF)

## AUTHOR INFORMATION


### Corresponding Author

**Murugappan Muthukumar** − *Department of Polymer Science and Engineering, University of Massachusetts, Amherst, Massachusetts 01003, United States;* orcid.org/0000-0001-7872-4883; Email: muthu@polysci.umass.edu

### Author

**Shibananda Das** − *Department of Polymer Science and Engineering, University of Massachusetts, Amherst, Massachusetts 01003, United States;* orcid.org/0000-0001-7694-0654

Complete contact information is available at: https://pubs.acs.org/10.1021/acs.macromol.2c01954


### Notes

The authors declare no competing financial interest.

## ACKNOWLEDGMENTS

This research was supported by the National Science Foundation (Grant DMR-2015935) and AFOSR (Grant FA 9550-20-1-0142).

## REFERENCES


(1) Liu, J.; Yang, R. Length-dependent thermal conductivity of single extended polymer chains. *Phys. Rev. B* **2012**, *86*, 104307.

(2) Henry, A.; Chen, G. High thermal conductivity of single polyethylene chains using molecular dynamics simulations. *Physical review letters* **2008**, *101*, 235502.

(3) Duan, X.; Li, Z.; Liu, J.; Chen, G.; Li, X. Roles of kink on the thermal transport in single polyethylene chains. *J. Appl. Phys.* **2019**, *125*, 164303.

(4) Zhang, T.; Wu, X.; Luo, T. Polymer nanofibers with outstanding thermal conductivity and thermal stability: Fundamental linkage between molecular characteristics and macroscopic thermal properties. *J. Phys. Chem. C* **2014**, *118*, 21148−21159.

(5) He, J.; Kim, K.; Wang, Y.; Liu, J. Strain effects on the anisotropic thermal transport in crystalline polyethylene. *Appl. Phys. Lett.* **2018**, *112*, 051907.

(6) Xiong, X.; Yang, M.; Liu, C.; Li, X.; Tang, D. Thermal conductivity of cross-linked polyethylene from molecular dynamics simulation. *J. Appl. Phys.* **2017**, *122*, 035104.

(7) Wang, X.; Ho, V.; Segalman, R. A.; Cahill, D. G. Thermal conductivity of high-modulus polymer fibers. *Macromolecules* **2013**, *46*, 4937−4943.

(8) Shen, S.; Henry, A.; Tong, J.; Zheng, R.; Chen, G. Polyethylene nanofibres with very high thermal conductivities. *Nat. Nanotechnol.* **2010**, *5*, 251−255.

(9) Choy, C.; Wong, Y.; Yang, G.; Kanamoto, T. Elastic modulus and thermal conductivity of ultradrawn polyethylene. *J. Polym. Sci., Part B: Polym. Phys.* **1999**, *37*, 3359−3367.

(10) Zhong, Z.; Wingert, M. C.; Strzalka, J.; Wang, H.-H.; Sun, T.; Wang, J.; Chen, R.; Jiang, Z. Structure-induced enhancement of thermal conductivities in electrospun polymer nanofibers. *Nanoscale* **2014**, *6*, 8283−8291.

(11) Zhu, B.; Liu, J.; Wang, T.; Han, M.; Valloppilly, S.; Xu, S.; Wang, X. Novel polyethylene fibers of very high thermal conductivity enabled by amorphous restructuring. *ACS omega* **2017**, *2*, 3931−3944.

(12) Ronca, S.; Igarashi, T.; Forte, G.; Rastogi, S. Metallic-like thermal conductivity in a lightweight insulator: solid-state processed ultra high molecular weight polyethylene tapes and films. *Polymer* **2017**, *123*, 203−210.

(13) Xu, Y.; Kraemer, D.; Song, B.; Jiang, Z.; Zhou, J.; Loomis, J.; Wang, J.; Li, M.; Ghasemi, H.; Huang, X.; Li, X.; Chen, G. others Nanostructured polymer films with metal-like thermal conductivity. *Nat. Commun.* **2019**, *10*, 1−8.

(14) Lu, T.; Kim, K.; Li, X.; Zhou, J.; Chen, G.; Liu, J. Thermal transport in semicrystalline polyethylene by molecular dynamics simulation. *J. Appl. Phys.* **2018**, *123*, 015107.

(15) He, J.; Liu, J. Molecular dynamics simulation of thermal transport in semicrystalline polyethylene: Roles of strain and the crystalline-amorphous interphase region. *J. Appl. Phys.* **2021**, *130*, 225101.

(16) Choy, C.; Young, K. Thermal conductivity of semicrystalline polymers—a model. *Polymer* **1977**, *18*, 769−776.

(17) Hennig, J. Anisotropy and structure in uniaxially stretched amorphous high polymers. *Journal of Polymer Science Part C: Polymer Symposia.* **1967**, *16*, 2751−2761.

(18) Takayanagi, M.; Imada, K.; Kajiyama, T. Mechanical properties and fine structure of drawn polymers. *Journal of Polymer Science Part C: Polymer Symposia* **1967**, *15*, 263−281.

(19) Liu, J.; Yang, R. Tuning the thermal conductivity of polymers with mechanical strains. *Phys. Rev. B* **2010**, *81*, 174122.

(20) Zhang, T.; Luo, T. Morphology-influenced thermal conductivity of polyethylene single chains and crystalline fibers. *J. Appl. Phys.* **2012**, *112*, 094304.

(21) Sasikumar, K.; Keblinski, P. Effect of chain conformation in the phonon transport across a Si-polyethylene single-molecule covalent junction. *J. Appl. Phys.* **2011**, *109*, 114307.

(22) Iyer, K.; Margossian, M.; Muthukumar, M. Interlude of metastability in the melting of polymer crystals. *J. Chem. Phys.* **2019**, *151*, 124903.

(23) Wang, S.-c.; Liang, X.-g.; Xu, X.-h.; Ohara, T. Thermal conductivity of silicon nanowire by nonequilibrium molecular dynamics simulations. *J. Appl. Phys.* **2009**, *105*, 014316.

(24) Lukes, J. R.; Zhong, H. Thermal conductivity of individual single-wall carbon nanotubes. *Journal of Heat Transfer* **2007**, *129*, 705−716.

(25) Sekimoto, K. Langevin equation and thermodynamics. *Prog. Theor. Phys. Suppl.* **1998**, *130*, 17−27.

(26) Harada, T.; Sasa, S.-i. Energy dissipation and violation of the fluctuation-response relation in nonequilibrium Langevin systems. *Phys. Rev. E* **2006**, *73*, 026131.

(27) Ditlevsen, P. D.; Stoltze, P.; No/rskov, J. K. Anharmonicity and disorder on the Cu (110) surface. *Phys. Rev. B* **1991**, *44*, 13002.

(28) Carlborg, C. F.; Shiomi, J.; Maruyama, S. Thermal boundary resistance between single-walled carbon nanotubes and surrounding matrices. *Phys. Rev. B* **2008**, *78*, 205406.

(29) Thomas, J. A.; Turney, J. E.; Iutzi, R. M.; Amon, C. H.; McGaughey, A. J. Predicting phonon dispersion relations and lifetimes from the spectral energy density. *Phys. Rev. B* **2010**, *81*, 081411.

(30) Hu, S.; Zhang, Z.; Wang, Z.; Zeng, K.; Cheng, Y.; Chen, J.; Zhang, G. Significant reduction in thermal conductivity of lithium cobalt oxide cathode upon charging: propagating and non-propagating thermal energy transport. *ES Energy & Environment* **2018**, *1*, 74−79.

(31) Wang, X.; Kaviany, M.; Huang, B. Phonon coupling and transport in individual polyethylene chains: a comparison study with the bulk crystal. *Nanoscale* **2017**, *9*, 18022−18031.

(32) Parker, S. F.; Braden, D. A.; Tomkinson, J.; Hudson, B. S. Full longitudinal acoustic mode (LAM) spectrum of an n-alkane: Comparison of observed and computed incoherent inelastic neutron scattering spectrum of n-octadecane. *J. Phys. Chem. B* **1998**, *102*, 5955−5956.

(33) Tomkinson, J.; Parker, S. F.; Braden, D. A.; Hudson, B. S. Inelastic neutron scattering spectra of the transverse acoustic modes of the normal alkanes. *Phys. Chem. Chem. Phys.* **2002**, *4*, 716−721.

(34) Basile, G.; Delfini, L.; Lepri, S.; Livi, R.; Olla, S.; Politi, A. Anomalous transport and relaxation in classical one-dimensional models. *European Physical Journal Special Topics* **2007**, *151*, 85−93.

(35) Giri, A.; Hopkins, P. E. A review of experimental and computational advances in thermal boundary conductance and nanoscale thermal transport across solid interfaces. *Adv. Funct. Mater.* **2020**, *30*, 1903857.
(36) Pollack, G. L. Kapitza resistance. *Reviews of modern physics* **1969**, *41*, 48.
(37) Lee, C.; Vanderbilt, D.; Laasonen, K.; Car, R.; Parrinello, M. Ab initio studies on the structural and dynamical properties of ice. *Phys. Rev. B* **1993**, *47*, 4863.
(38) Landry, E.; McGaughey, A. Thermal boundary resistance predictions from molecular dynamics simulations and theoretical calculations. *Phys. Rev. B* **2009**, *80*, 165304.
(39) Aubry, S.; Kimmer, C. J.; Skye, A.; Schelling, P. K. Comparison of theoretical and simulation-based predictions of grain-boundary Kapitza conductance in silicon. *Phys. Rev. B* **2008**, *78*, 064112.
(40) Schelling, P.; Phillpot, S.; Keblinski, P. Phonon wave-packet dynamics at semiconductor interfaces by molecular-dynamics simulation. *Appl. Phys. Lett.* **2002**, *80*, 2484−2486.
(41) Tian, Z.; White, B., Jr.; Sun, Y. Phonon wave-packet interference and phonon tunneling based energy transport across nanostructured thin films. *Appl. Phys. Lett.* **2010**, *96*, 263113.
(42) Wei, X.; Luo, T. A phonon wave packet study of thermal energy transport across functionalized hard-soft interfaces. *J. Appl. Phys.* **2019**, *126*, 015301.
(43) Stevens, R. J.; Zhigilei, L. V.; Norris, P. M. Effects of temperature and disorder on thermal boundary conductance at solid−solid interfaces: Nonequilibrium molecular dynamics simulations. *Int. J. Heat Mass Transfer* **2007**, *50*, 3977−3989.


https://doi.org/10.1021/acs.macromol.2c01954
*Macromolecules* 2023, 56, 393−403